J|A|C|S
ARTICLES

Published on Web 02/15/2010

Pd Nanoparticles Embedded into a Metal-Organic Framework: Synthesis, Structural Characteristics, and Hydrogen Sorption Properties

Claudia Zlotea,[†] Renato Campesi,[†] Fermin Cuevas,[†] Eric Leroy,[†] Philippe Dibandjo,[‡] Christophe Volkringer,[§] Thierry Loiseau,[§] Gérard Férey,[§] and Michel Latroche*,[†]

Institut de Chimie et des Materiaux de Paris-Est, CNRS UMR 7182, 2-8, Rue Henri Dunant, 94320 Thiais, France, Institut de Sciences des Matériaux de Mulhouse, CNRS, 15, Rue Jean Starcky, 68057 Mulhouse, France, and Institut Lavoisier, UMR CNRS 8180, Université de Versailles Saint Quentin, 45, Avenue des Etats-Unis, 78035 Versailles Cedex, France

Received October 15, 2009; E-mail: michel.latroche@icmpe.cnrs.fr

Abstract: The metal-organic framework MIL-100(Al) has been used as a host to synthesize Pd nanoparticles (around 2.0 nm) embedded within the pores of the MIL, showing one of the highest metal contents (10 wt %) without degradation of the porous host. Textural properties of MIL-100(Al) are strongly modified by Pd insertion, leading to significant changes in gas sorption properties. The loss of excess hydrogen storage at low temperature can be correlated with the decrease of the specific surface area and pore volume after Pd impregnation. At room temperature, the hydrogen uptake in the composite MIL-100(Al)/Pd is almost twice that of the pristine material. This can be only partially accounted by Pd hydride formation, and a "spillover" mechanism is expected to take place promoting the dissociation of molecular hydrogen at the surface of the metal nanoparticles and the diffusion of monatomic hydrogen into the porosity of the host metal-organic framework.

Introduction

Since their discovery in 1989,[1] crystallized porous coordination polymers (PCP) also labeled metal-organic frameworks (MOFs) are more and more topical.[2,3] This new class of multifunctional materials associates, by exclusively strong bonds, a large variety of organic linkers (mostly polytopic) and metallic moieties. Rigid or flexible,[4,5] the numerous resulting frameworks often offer large and tunable cavities, high surface area, controlled porosity, and low density. As shown in some recent reviews, these characteristics, enhanced by the possibilities of functionalization on both the organic and inorganic parts,[6,7] are interesting for applications mainly in the domains of gas separation/storage,[2,8−11] and more recently, drug delivery.[14] catalysis,[12,13−16] A recent themed issue develops all of these aspects.[17]

These exceptional properties of MOFs induced many studies on hydrogen storage[18,19] Unfortunately, whereas MOFs display high hydrogen uptake at low temperatures (currently 7.5 wt % at 7 MPa),[19] this value is lower than 1 wt % at room temperature and close to values of other porous materials such as nanostructured carbons[20−25] and zeolites.[26−28] These poor perfor-

[†] Institut de Chimie et des Materiaux de Paris-Est.
[‡] Institut de Sciences des Matériaux de Mulhouse.
[§] Université de Versailles Saint Quentin.

(1) Hoskins, B. F.; Robson, R. *J. Am. Chem. Soc.* **1989**, *111*, 5962–5964.
(2) Férey, G. *Chem. Soc. Rev.* **2008**, *37*, 191–214.
(3) Kitagawa, S.; Kitaura, R.; Noro, S.-I. *Angew. Chem., Int. Ed.* **2004**, *43*, 2334–2375.
(4) Rowsell, J. L. C.; Yaghi, O. M. *Microporous Mesoporous Mater.* **2004**, *73*, 3–14.
(5) Férey, G.; Serre, C. *Chem. Soc. Rev.* **2009**, *38*, 1380–1399.
(6) Wang, Z.; Cohen, S. M. *Chem. Soc. Rev.* **2009**, *38*, 1315–1329.
(7) Dincă, M.; Dailly, A. *J. Am. Chem. Soc.* **2006**, *128*, 16876–16883.
(8) Lin, X.; Jia, J.; Hubberstey, P.; Schröder, M.; Champness, N. R. *CrystEngComm* **2007**, *9*, 438–448.
(9) Collins, D. J.; Zhou, H.-C. *J. Mater. Chem.* **2007**, *17*, 3154–3160.
(10) Dincă, M.; Long, J. R. *Angew. Chem., Int. Ed.* **2008**, *47*, 6766–6779.
(11) Li, J.-R.; Kuppler, R. J.; Zhou, H.-C. *Chem. Soc. Rev.* **2009**, *38*, 1477–1504.
(12) Ma, L.; Abney, C.; Lin, W. *Chem. Soc. Rev.* **2009**, *38*, 1248–1256.
(13) Lee, J.-Y.; Farha, O. K.; Roberts, J.; Scheidt, K. A.; Nguyen, S. T.; Hupp, J. T. *Chem. Soc. Rev.* **2009**, *38*, 1450–1459.
(14) Horcajada, P.; Serre, C.; Maurin, G.; Ramsahye, N. A.; Balas, F.; Vallet-Regi, M.; Sebban, M.; Taulelle, F.; Férey, G. *J. Am. Chem. Soc.* **2008**, *130*, 6774–6780.
(15) Horcajada, P.; Serre, C.; Vallet-Regi, M.; Sebban, M.; Taulelle, F.; Férey, G. *Angew. Chem., Int. Ed.* **2006**, *45*, 5974–5978.
(16) Rieter, W. J.; Pott, K. M.; Taylor, K. M. L.; Lin, W. *J. Am. Chem. Soc.* **2008**, *130*, 11584–11585.
(17) Long, J. R.; Yaghi, O. M. *Chem. Soc. Rev.* **2009**, *38*, 1213–1504.
(18) Murray, L. J.; Dincă, M.; Long, J. R. *Chem. Soc. Rev.* **2009**, *38*, 1294–1314.
(19) Wong-Foy, A. G.; Matzger, A. J.; Yaghi, O. M. *J. Am. Chem. Soc.* **2006**, *128*, 3494–3495.
(20) Thomas, K. M. *Catal. Today* **2007**, *120*, 389–398.
(21) Panella, B.; Hirscher, M. *Carbon* **2005**, *43*, 2209–2214.
(22) Poirier, E.; Chahine, R.; Bénard, P.; Cossement, D.; Lafi, L.; Mélançon, E.; Bose, T. K.; Désilets, S. *Appl. Phys. A: Mater. Sci. Process.* **2004**, *78*, 961–967.
(23) Zhou, L.; Zhou, Y.; Sun, Y. *Int. J. Hydrogen Energy* **2004**, *29*, 319–322.
(24) De, La.; Casa-Lillo, M. A.; Lamari-Darkrim, F.; Cazorla-Amorós, D.; Linares-Solano, A. *J. Phys. Chem. B* **2002**, *106*, 10930–10934.
(25) Gadiou, R.; Saadallah, S.-E.; Piquero, T.; David, P.; Parmentier, J.; Vix-Guterl, C. *Microporous Mesoporous Mater.* **2005**, *79*, 121–128.
(26) Jhung, S. H.; Lee, J. S.; Yoon, J. W.; Kim, D. P.; Chang, J. S. *Int. J. Hydrogen Energy* **2007**, *32*, 4233–4237.

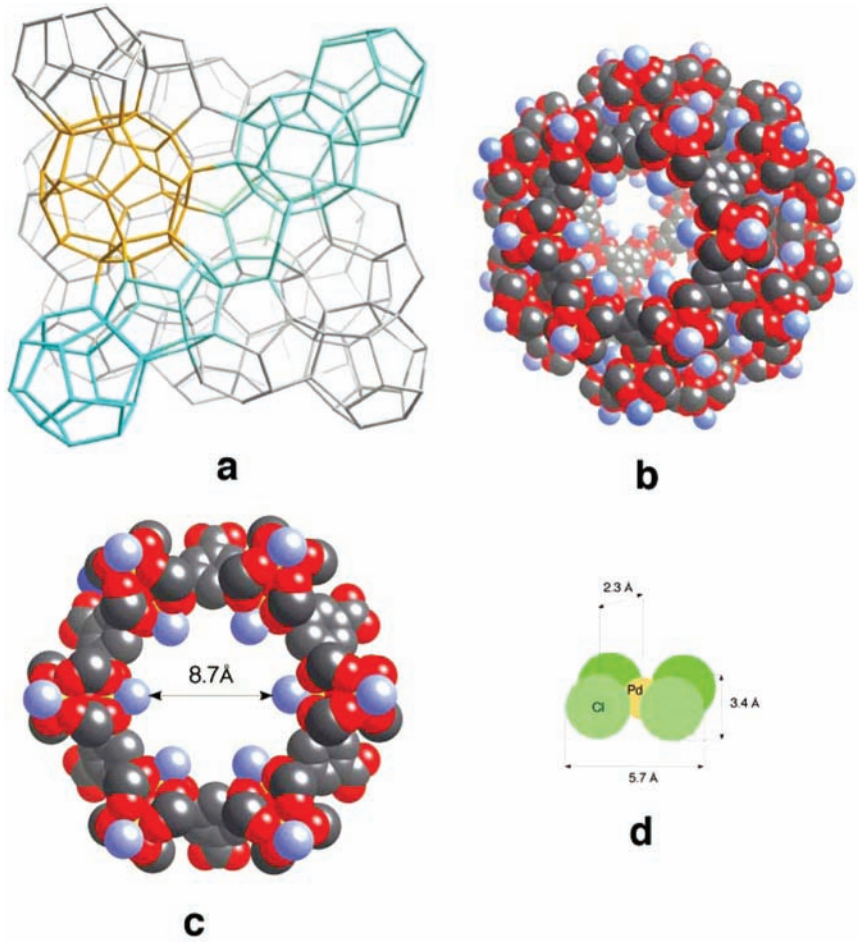

Figure 1. (a) The MTN topology of MIL-100(Al): large cages in yellow and small ones in turquoise. (b) Space-filling perspective view of the large cage of MIL-100(Al): carbon in gray, oxygen in red, terminal groups (water or OH) in pale blue. (c) Space-filling representation of the hexagonal window of the large cage (same color codes as in panel b). (d) Steric hindrance of the $[PdCl_4]$ anion at the same scale.

mances at 300 K can be explained by the weak interactions (in the range 3−10 kJ mol^{-1}) between H_2 molecules and the frameworks. Besides optimizing the size of the pores by using interpenetrated or interwoven solids, different strategies are currently applied for enhancing hydrogen adsorption energies in MOFs at room temperature. The first uses exposed metal sites of the framework.[10,29,30] The second exploits the "spillover' effect (catalyzed formation of monoatomic hydrogen), created either by incorporating metal catalysts in the pores[31,32] or, through a "cascade" mechanism, by mixing the carbon-supported catalyst with the MOF.[33−35] Monoatomic hydrogen, formed on the catalyst, migrates first on the carbon support before going on the MOF. However, the mechanistic details of the hydrogen "spillover" on metals, not even considering the support, are poorly understood. The last strategy aims at introducing cations[36,37] or generating noble metals within the cavities after impregnation and further reduction of the incorporated precursor,[38−40] in order to achieve either better interactions or formation of hydrides.

This last method of in situ metallic cluster generation is applied to MIL-100(Al) (MIL stands for Materials of Institut Lavoisier) to see its effect on hydrogen storage at ambient temperature. MIL-100 structure (metal trimesate)[41] is currently one of the rare crystallized mesoporous solids (Figure 1), which exhibits both very large pores and large specific surface areas.

(27) Dong, J.; Wang, X.; Xu, H.; Zhao, Q.; J., L. *Int. J. Hydrogen Energy* **2007**, *32*, 4998–5004.
(28) Langmi, H. W.; Walton, A.; Al-Mamouri, M. M.; Johnson, S. R.; Book, D.; Speight, J. D.; Edwards, P. P.; Gameson, I.; Anderson, P. A.; Harris, I. R. *J. Alloys Compd.* **2003**, *356*−*357*, 710–715.
(29) Wang, X.-S.; Ma, S.; Forster, P. M.; Yuan, D.; Eckert, J.; Lopez, J. J.; Murphy, B. J.; Parise, J. B.; Zhou, H.-C. *Angew. Chem., Int. Ed.* **2008**, *47*, 7263–7266.
(30) Lee, Y.-G.; Moon, H. R.; Cheon, Y. E.; Suh, M. P. *Angew. Chem., Int. Ed.* **2008**, *47*, 7741–7745.
(31) Sabo, M.; Henschel, A.; Froede, H.; Klemm, E.; Kaskel, S. *J. Mater. Chem.* **2007**, *17*, 3827–3832.
(32) Cheon, Y. E.; Paik Suh, M. *Angew. Chem., Int. Ed.* **2009**, *48*, 2899–2903.
(33) Li, Y.; Yang, R. *J. Am. Chem. Soc.* **2006**, *128*, 726–727.
(34) Liu, Y. Y.; Zeng, J. L.; Zhang, J.; Xu, F.; XSun, L. X. *Int. J. Hydrogen Energy* **2007**, *32*, 4005–4010.
(35) Tsao, C. S.; Yu, M. S.; Wang, C. Y.; Liao, P. Y.; Chen, H. L.; Jeng, U. S.; Tzeng, Y. R.; Chung, T. Y.; Wu, H.-C. *J. Am. Chem. Soc.* **2009**, *131*, 1404–1406.
(36) Mulfort, K. L.; Hupp, J. T. *J. Am. Chem. Soc.* **2007**, *129*, 9604–9605.
(37) Mulfort, K. L.; Hupp, J. T. *Inorg. Chem.* **2008**, *47*, 7936–7938.
(38) Hermes, S.; Schröter, M.-K.; Schmid, R.; Jhodeir, L.; Muhler, M.; Tissler, A.; Fischer, R. W.; Fischer, R. A. *Angew. Chem., Int. Ed.* **2005**, *44*, 6237–6241.
(39) Hwang, Y. K.; Hong, D.-Y.; Chang, J.-S.; Jhung, S. H.; Seo, Y.-K.; Kim, J.; Vimont, A.; Daturi, M.; Serre, C.; Férey, G. *Angew. Chem., Int. Ed.* **2008**, *47*, 4144–4148.
(40) Esken, D.; Zhang, X.; Lebedev, O. I.; Schröder, F.; Fischer, R. A. *J. Mater. Chem.* **2009**, *19*, 1314–1319.
(41) Férey, G.; Serre, C.; Millange, F.; Mellot-Draznieks, C.; Surblé, S.; Dutour, J.; Margiolaki, I. *Angew. Chem., Int. Ed.* **2004**, *43*, 6296–6301.

For instance, MIL-101, the isotypic homologue of MIL-100 with terephtalate anions,[42] possesses a specific surface area up to 5500 $m^2\ g^{-1}$ and hydrogen uptake of 6.1 wt % at 77 K and 6 MPa.[43] The MIL-100 topology results from the association of 1,3,5-benzenetricarboxylate (or BTC) ions with μ_3-oxo-centered trinuclear units of octahedrally coordinated trivalent metals (M^{III} = Cr,[41] Fe,[44] Al[45]). Their 3D connexion provides an open framework, derived from the cubic zeolitic MTN topology,[46] with two types of extra-large cavities, determined by 20 and 28 trimers (effective internal diameters: 2.1 and 2.5 nm, respectively, for MIL-100). Whereas the small cages are limited exclusively by pentagonal windows, the large ones have also hexagonal ones that allow better access to the center of the cages for the guest molecules.

As a contribution to the domain of hydrogen storage and its eventual improvement at room temperature, the present work will report and discuss on the synthesis, the structural characterizations and the hydrogen sorption properties of both the new metal-organic framework MIL-100(Al) and the composite material formed by generation of Pd nanoparticles in MIL-100(Al).

Experimental Section

The aluminum trimesate MIL-100(Al) was obtained following the synthesis procedure described in the literature.[45] A careful activation of the as-synthesized solid (600 K under dynamic vacuum overnight) was performed before impregnation. To generate Pd nanoparticles into the MIL-100(Al) porosity, a chemical wetting procedure, already applied for producing carbon replica/Pd composites, was used.[47] A solution of tetrachloropalladinic acid (H_2PdCl_4) was prepared by mixing 0.3353 g of $PdCl_2$ (Alfa Caesar, purity 99.9%) into 20 mL of 10% v/v HCl aqueous solution under stirring at 300 K until complete dissolution. The activated MIL-100(Al) in powder form was then impregnated with the tetrachloropalladinic acid solution for a final Pd concentration of 10 wt %. The mixture of powder and solution was stirred for 3 h and dried under air at 330 K. The $PdCl_4^{2-}$ ions were reduced by heating the impregnated MIL-100(Al) in a Ar/H_2 flow (0.5 L min^{-1}) at 553 K for 6 h. The sample was then outgassed under secondary vacuum for 11 h at 553 K.

The chemical composition of the impregnated material was determined by an inductively coupled plasma optical emission spectrometer (ICP-OES). The measured Pd content is 9.7 wt %, in agreement with the nominal composition. This material will hereafter be named MIL-100(Al)/Pd.

Structural characterization of MIL-100(Al) and MIL-100(Al)/Pd were performed by X-ray diffraction (XRD) using a Bruker D8 Advance instrument (Cu Kα, Bragg−Brentano geometry, backscattered rear graphite monochromator). To characterize the crystallographic changes induced by hydrogen absorption in MIL-100(Al)/Pd, in situ XRD measurements were performed at room temperature at various increasing hydrogen pressures. The sample was initially evacuated under primary vacuum, and hydrogen pressure was incremented by steps up to 10 kPa.

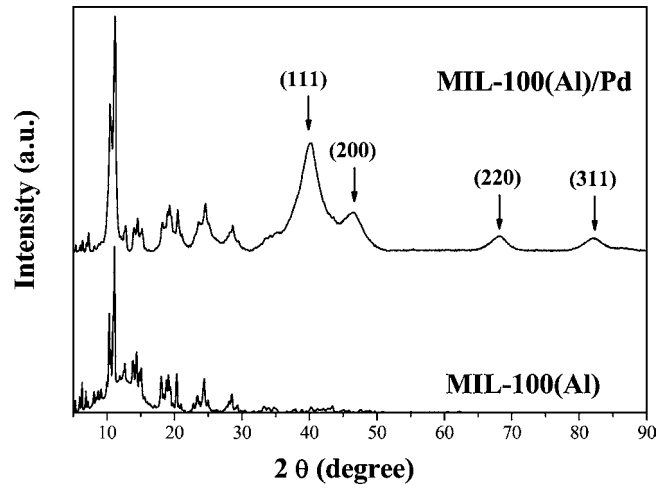

Figure 2. Comparison of XRD patterns of MIL-100(Al) (bottom) and MIL-100(Al)/Pd (top). The diffraction peaks and corresponding Miller indices of Pd *fcc* crystal structure are also displayed.

Microstructural analyses were performed by scanning electron microscopy (SEM-LEO 1530 with a field emission gun) and transmission electron microscopy (TEM-Tecnai F20 with a field emission gun 200 KV, punctual resolution 0.24 nm and energy filtering GIF).

The textural properties were determined from nitrogen adsorption/desorption isotherms measured with a Micromeritics ASAP 2020 instrument. The specific surface area was obtained by the Brunauer−Emmett−Teller (BET) method, the total pore volume was computed from the amount of gas adsorbed at $p/p_0 = 0.99$, and the micropore volume was calculated using the Dubinin−Radushkevich equation in the relative pressure range 10^{-4} to 10^{-2}.

Hydrogen sorption properties were determined by measuring the pressure−composition isotherms (PCI) at 77 and 298 K up to 8 MPa. The PCI curves are recorded using a volumetric device (Sievert's method) equipped with calibrated and thermostatted volumes and pressure gauges.[48] The samples are enclosed in a stainless steel sample holder closed with a metal seal. Before any sorption measurements, the samples are outgassed under primary vacuum at 473 K for 10 h. The sample holder is immersed in a liquid N_2 Dewar at 77 K or in a thermostatted water bath maintained at 298 K, and high purity hydrogen (6 N) is introduced step by step up to 8 MPa. The pressure variations due to both gas cooling and hydrogen adsorption are measured after reaching thermodynamic equilibrium, usually in the range of minutes. Real equation of state for hydrogen gas is used from the program GASPAK V3.32.[49] The PCI curves are measured twice (i.e., two full adsorption−desorption cycles) in order to check the hysteresis effect and the measurement repeatability. All capacities reported here refer to the sample dry mass (i.e., outgassed mass). Sample volume correction is derived from density measurement obtained with a helium AccuPyc 1330 Micromeritics pycnometer. Using this method, the measured densities of MIL-100(Al) and MIL-100(Al)/Pd are 1.77 ± 0.09 and 1.81 ± 0.09 g cm^{-3}, respectively.

Results

The X-ray powder diagram of MIL-100(Al) (Figure 2 bottom) is in excellent agreement with the data extracted from a recent single crystal determination.[45] Beside a slight modification of

(42) Férey, G.; Mellot-Draznieks, C.; Serre, C.; Millange, F.; Dutour, J.; Surblé, S.; Margiolaki, I. *Science* **2005**, *309*, 2040–2042.
(43) Latroche, M.; Surblé, S.; Serre, C.; Mellot-Draznieks, C.; Llewellyn, P. L.; Chang, J.-S.; Jhung, S.-H.; Férey, G. *Angew. Chem., Int. Ed.* **2006**, *45*, 8227–8231.
(44) Horcajada, P.; Surblé, S.; Serre, C.; Hong, D.-Y.; Seo, Y.-K.; Chang, J.-S.; Grenèche, J.-M.; Margiolaki, I.; Férey, G. *Chem. Commun* **2007**, *2820*, 2822.
(45) Volkringer, C.; Popov, D.; Loiseau, T.; Férey, G.; Burghammer, M.; Riekel, C.; Haouas, M.; Taulelle, F. *Chem. Mater.* **2009**, *21*, 5695–5697.
(46) Schlenker, J. L.; Dwyer, F. G.; Jenkins, E. E.; Rohrbaugh, W. J.; Kokotailo, G. T. *Nature* **1981**, *294*, 340–342.
(47) Campesi, R.; Cuevas, F.; Gadiou, R.; Leroy, E.; Hirscher, M.; Vix-Guterl, C.; Latroche, M. *Carbon* **2008**, *46*, 206–214.
(48) Sieverts, A. *Z. Phys. Chem.* **1907**, *60*, 129–201.
(49) Lemmon, E. W.; Peskin, A. P.; McLinden, M. O.; Friend, D. G. *NIST12 Thermodynamic and Transport Properties of Pure Fluids V5.0*; NIST: Gaithersburg, MD, 2000.

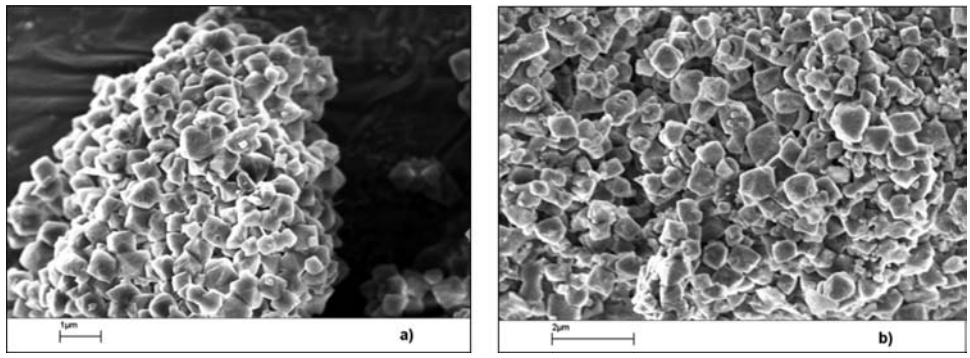

Figure 3. SEM images showing the crystal morphology of MIL-100(Al) (a) and MIL-100(Al)/Pd (b).

the diffraction peak intensities of the host MIL-100(Al), the XRD pattern of the MIL-100(Al)/Pd solid (Figure 2, top) shows four additional peaks at $2\theta = 40.2°$, 46.5°, 68.2°, and 81.1°, which can be ascribed to the (111), (200), (220), and (310) reflections of a Pd cubic cell (*Fm*-3*m*) (α-phase) with a lattice constant equal to $a = 3.90 \pm 0.01$ Å. This clearly indicates the biphasic nature of MIL-100(Al)/Pd, which will be called a composite in the following. As calculated by Scherrer's formula, the mean size of the Pd nanoparticles is 2.5 ± 0.2 nm. These nanoparticles are small enough to occupy the two available mesoporous cavities into the MIL-100(Al) crystal structure.

The scanning electron microscopy (SEM) images show (Figure 3a,b) that both samples are formed by octahedral crystals with size ranging between 0.2 and 0.8 μm, proving that the Pd insertion does not change the microstructural properties of MIL-100(Al). Moreover, bright field transmission electron microscopy images (Figure 4a) acquired on two crystals of the MIL-100(Al)/Pd composite show black spots that are attributed to the Pd nanoparticles. Their dispersion is clearly observed in the dark field scanning transmission image (Figure 4b). Taking into account that in a dark field scanning transmission image the heaviest elements (high *Z* value) appear brighter, the white spots can be reasonably attributed to the Pd nanoparticles, in agreement with the electron dispersion X-ray spectroscopy analysis (not shown). The particle size distribution as determined from the STEM image is displayed in Figure 4c. The mean particle size (1.8 ± 0.4 nm) is in agreement with the value obtained from the Scherrer formula (2.5 ± 0.2 nm). Few Pd nanoparticles have sizes between 6 and 8 nm, larger than the available mesopores, and presumably they are laying at the outer surface of the host structure. A simple calculation based on the distribution curve shown in Figure 4c allows us to estimate those particles at around 10%.

The N_2 adsorption/desorption isotherms of MIL-100(Al) and MIL-100(Al)/Pd at 77 K show (Figure 5) a mixture of type I and IV curves.[50] For MIL-100(Al), the steep increase in the adsorbed volume at low relative pressure relates to microporosity, and the slight secondary uptake points to the existence of mesopores. The adsorption/desorption hysteresis loop for MIL-100(Al)/Pd denotes the existence of developed mesoporosity, while the final almost vertical tail at relative pressure near $p/p_0 = 1.0$ indicates the presence of macroporosity. The textural parameters (Table 1) show that the specific surface areas calculated by the BET method are 1200 and 380 $m^2\ g^{-1}$ for MIL-100(Al) and MIL-100(Al)/Pd, respectively. Using the

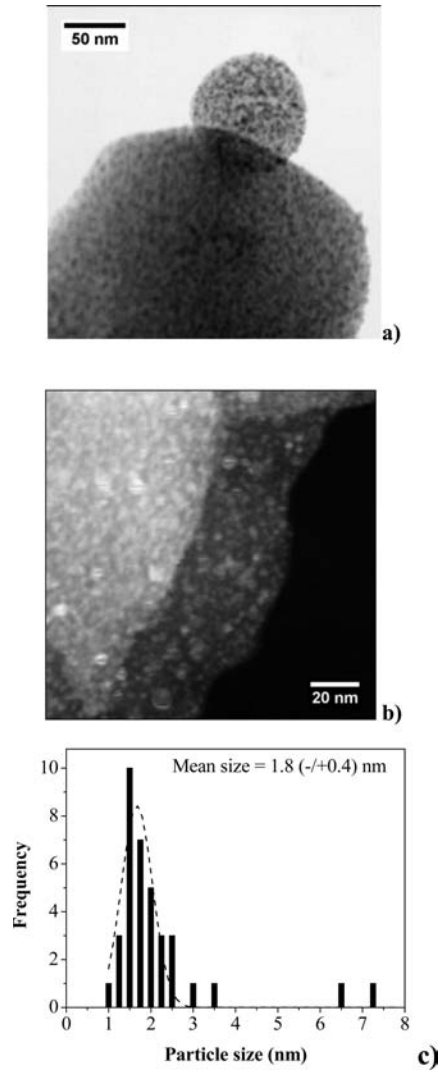

Figure 4. TEM bright field (a) and STEM dark field (b) images of the MIL-100(Al)/Pd composite. (c) The particle size distribution as determined from STEM image.

Dubinin−Radushkevich equation, the micropore volumes of MIL-100(Al) and MIL-100(Al)/Pd are 0.40 and 0.12 $cm^3\ g^{-1}$, respectively. The total pore volumes, as calculated from the adsorption value at relative pressure $p/p_0 = 0.99$, are 0.65 and 0.33 $cm^3\ g^{-1}$ for MIL-100(Al) and MIL-100(Al)/Pd, respectively. The decrease of specific surface area, micropore, and total volumes indicates that the insertion of Pd nanoparticles modifies the pore structure of the pristine MIL-100(Al).

(50) Rouquerol, J.; Avnir, D.; Fairbridge, C. W.; Everett, D. H.; Haynes, J. H.; Pernicone, N.; Ramsay, J. D. F.; Sing, K. S. W.; Unger, K. K. *Pure Appl. Chem.* **1999**, *1*, 1739–1758.

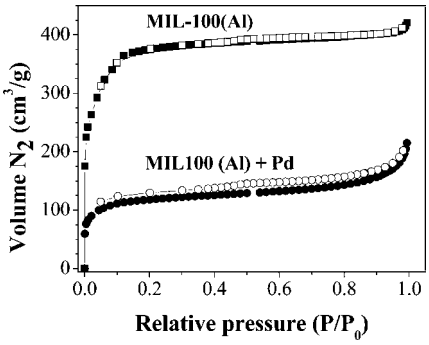

Figure 5. Comparison of N_2 adsorption (solid symbols) and desorption (open symbols) isotherms at 77 K of the MIL-100(Al) (top) and MIL-100(Al)/Pd (bottom).

The hydrogen sorption properties of the MIL-100(Al) and MIL-100(Al)/Pd composite have been determined with a good repeatability by measuring the Gibbs excess sorption isotherms at 77 and 298 K (Figure 6a,b). No adsorption/desorption hysteresis is observed for both samples. At 77 K, the excess sorption isotherms display a type I trend typical for monolayer adsorption on microporous materials.[50] The maximum hydrogen capacities at 77 and 298 K and 4 MPa of both MIL-100(Al) and MIL-100(Al)/Pd are listed in Table 1. The Pd insertion decreases the excess adsorption capacity at 77 K. On the contrary, other authors have reported an enhancement of hydrogen uptake in MOF/Pd composites at 77 K,[31,32] though their experiments were performed at pressures below 0.1 MPa and for much lower Pd contents ($\leq$3 wt %) than the composite here presented. As for room temperature measurements, a larger hydrogen sorption is noticed for the MIL-100(Al)/Pd composite as compared to MIL-100(Al). The isotherm of the MIL-100(Al) at 298 K displays a linear trend typical for diluted monolayer adsorption (Henry type), as commonly reported for microporous materials at ambient temperature.[50] The isotherm of the MIL-100(Al)/Pd composite shows a steep increase at low pressure (below 0.1 MPa) followed by a constant increase with pressure and an almost similar slope as for the MIL-100(Al) isotherm. The different sorption properties at ambient temperature can be ascribed to the formation of Pd hydride for pressure below 0.1 MPa. To study the hydrogen absorption in the Pd nanoparticles, in situ XRD during hydrogen loading has been performed at room temperature up to 10 kPa (Figure 7). The XRD patterns of the sample under vacuum and for hydrogen pressure up to 0.5 kPa do not change significantly. Further increase of pressure up to 4.5 kPa induces a constant shift of the diffraction peaks toward lower 2θ angles demonstrating an expansion of the lattice parameters due to the hydrogen insertion at the interstitial sites of Pd. Since the very broad diffraction peaks are a convolution of the α- and β-phase contributions, a clear identification of the pressure value for which the Pd β-hydride starts to form is rather difficult. Nevertheless, the formation of the Pd β-hydride is complete at 4.5 kPa and the exposure to higher pressure induces no significant changes of the XRD patterns. The

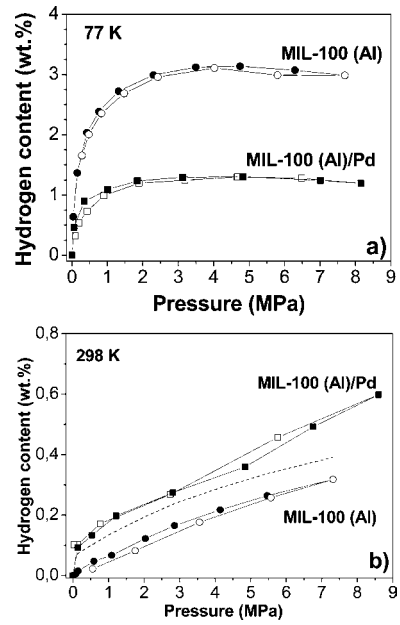

Figure 6. Comparison of H_2 adsorption (solid symbols) and desorption (open symbols) isotherms at 77 K (a) and 298 K (b) of MIL-100(Al) and MIL-100(Al)/Pd. The dashed line in panel b is calculated from the addition of the quantity of H_2 required for the formation of the bulk β-Pd hydride (taken from ref 57) and the amount of physisorbed H_2 by Pd-free MIL-100(Al).

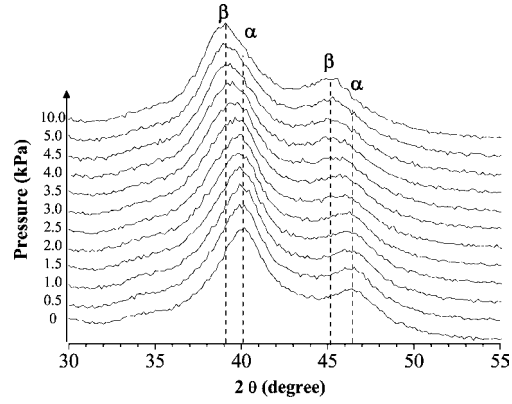

Figure 7. In situ XRD, during hydrogen absorption in Pd nanoparticles at room temperature and pressure up to 10 kPa. The α- and β-phase line positions are shown by straight lines in order to follow the phase transition during hydrogen absorption.

β-hydride phase has cubic structure similar to that of pure Pd with larger lattice parameter 3.99 $\pm$ 0.01 Å. The complete desorption of hydrogen from Pd nanoparticles is possible under primary vacuum, as demonstrated by the XRD measurements (not shown here).

Discussion

The following discussion will concern three points: (i) the loaded amount of Pd in various MOFs, (ii) the location of Pd

Table 1. Textural and Hydrogen Sorption Properties of MIL-100(Al) and MIL-100(Al)/Pd

Properties	MIL 100(Al)	MIL100(Al)/Pd
SS (BET) ($m^2\ g^{-1}$)	1200 ± 33	380 ± 8
$V_{0.99p}$ ($cm^3\ g^{-1}$)	0.65 ± 0.06	0.33 ± 0.03
$V_{\mu p}$ ($cm^3\ g^{-1}$)	0.40 ± 0.04	0.12 ± 0.01
excess hydrogen capacity (4 MPa, 77 K) (wt %)	3.1 ± 0.1	1.3 ± 0.1
excess hydrogen capacity (4 MPa, 298 K) (wt %)	0.19 ± 0.05	0.35 ± 0.05

nanoparticles in the composite MIL-100(Al)/Pd, and (iii) the hydrogen sorption properties of the pristine MIL-100(Al) and the MIL-100(Al)/Pd composite. With due recognition of the reported gas phase followed by photolysis of an MOF (up to 35% Pd),[40] the results presented here correspond to one of the highest (10 wt %) Pd-containing metal-organic frameworks produced by a chemical wetting procedure followed by reduction without degradation of the porous host. Usually, it does not exceed 3 wt %.[31,32,39] Pd nanoparticles (1 wt %) were successfully encapsulated in amine-grafted MIL-101 by ionic reactions of ammonium groups with anionic noble metal salt ($PdCl_4^{-2}$) and a further gentle reduction with $NaBH_4$.[39] The incipient wetness infiltration of a metal-organic precursor followed by reduction in vacuum or in H_2 flow produces MOF-5 impregnated with Pd nanoparticles (1 wt %).[31] However, the latter synthesis method partially decomposes the MOF-5 despite the low metal loading. Another way to embed Pd nanoparticles in a MOF is based on the autoredox reaction between the organic species incorporated in the solid and Pd ions.[32] This method can incorporate up to 3 wt % of Pd nanoparticles (3 nm) in a MOF in the absence of extra reducing agent. However, the main drawback of all of these synthesis methods is the low metal content that can be loaded in the MOF porosity without degradation.

The second point will address the localization of the Pd nanoparticles relative to the structure of the host material. Two locations can possibly host the Pd nanoparticles: the outer surface and the inner porosity of the MIL material.

Although both SEM and TEM techniques show that the macroscopic octahedral shape of the MIL-100(Al) crystals is preserved after the Pd insertion, several facts argue for the existence of particles within the cages: (i) the steric considerations of the chloropalladate ions that are wetting the pores of MIL-100(Al) during the synthesis, (ii) the drastic modification of the textural properties (BET surface area, total and micropore volumes) of MIL-100(Al)/Pd compared to those of MIL-100(Al) (Table 1), (iii) the slight evolution of the intensities of the Bragg peaks in MIL-100(Al)/Pd, and (iv) the observed densities of each phase.

Indeed, due to the method used, the fixation of precursors by impregnation can occur both on the surface of the grains and within the pores. This last possibility is closely conditioned to the size of the windows allowing access to the cages, the effective diameter of the pores being further a parameter determining the amount of trapped precursors and subsequently of nanoparticles after the reduction. The structure of MIL-100(Al) (Figure 1) exhibits two types of cages. The smaller one, with 20 vertices, has only pentagonal windows, with a free diameter of 5.4 Å. The large one, with 28 vertices, shows the same pentagonal windows but possesses also four hexagonal ones. Their free diameter (8.7 Å) is large enough to allow the penetration of the $[PdCl_4]^{2-}$ ions, the steric hindrance of which is $5.7 \times 5.7 \times 3.4$ Å^3 (Figure 1). Geometrically, this means that the $[PdCl_4]^{2-}$ ions can enter in the cages only through the hexagonal windows and not through the pentagonal ones. Using this static geometrical criterion, only the large cages with hexagonal windows can be filled with the chloropalladate ions precursor. However, the terminal water molecules linked to the Al_3O trimere of the pentagonal windows can dynamically exchange molecules in an aqueous solution and might allow the diffusion of the chloropalladate ions even within the small cages.

The changes of the specific surface area and micropore and total volumes (Table 1) clearly indicate that a part of the Pd nanoparticles is located within the porous structure of the host MIL-100(Al). The Pd nanoparticles laying on the surface of grains do not contribute to the textural properties. Nevertheless, the Pd nanoaggregates that are located inside the cages of the host material could block the access of N_2 molecules to the porosity and therefore decrease the overall textural values of the composite as compared to the host material.

Even if the effects are less spectacular, the slight variation of the intensities of the diffraction peaks belonging to the MIL-100(Al) in the XRD pattern of the MIL-100(Al)/Pd composite might confirm the existence of Pd nanoparticles within the pores of host material. One can consider that some Pd atoms located inside the cages of the host strongly bound to the internal surface of the cage and crystallographically belong to the structure and symmetry of MIL-100 and therefore participating to the structure factors of the Bragg peaks. The rest of Pd nanoaggregates have a size which is larger than the scattering coherent length and give rise to the diffraction peaks of the *fcc* crystal structure of Pd.

Another proof of the existence of Pd nanoparticles within the porosity of MIL-100(Al) is provided by the density measurements using the He pycnometer method. The measured densities are 1.77 and 1.81 g cm^{-3} for the MIL-100(Al) and MIL-100(AL)/Pd, respectively. If the composite is just a biphasic mixture of MIL-100(Al) (90 wt %) and metallic Pd (10 wt %) laying on the surface without insertion in the host porosity, the density of the synthesized material would be 1.93 g cm^{-3}, whereas 1.81 g cm^{-3} is measured experimentally. This reduction can only be explained by a decrease of the accessible porous volume probed by He pycnometry, i.e., an increase of the total volume occupied by the composite. This decrease of the accessible porous volume is directly linked to the presence of nanoparticles within the pores, which reduces the He access to the cavities. Moreover, the decrease of the porous volume noticed by He pycnometry is in conformity with the changes of the textural properties.

The synthesis product can be then clearly depicted as a combination of the pristine MIL-100(Al) and Pd nanoparticles. Few Pd nanoparticles are laying on the MIL surface whereas most of them are embedded in the pores of the MIL structure. This justifies the already mentioned composite nature of MIL-100(Al)/Pd.

Finally, the last point to be addressed in the present study is regarding the hydrogen sorption properties of the pristine MIL-100(Al) and the MIL-100(Al)/Pd composite.

At 77 K, the excess hydrogen capacities at 4 MPa are 3.1 and 1.3 wt % for MIL-100(Al) and MIL-100(Al)/Pd, respectively (Table 1). The hydrogen capacity of MIL-100(Al) is in good agreement with previously reported values for porous hybrid materials (2.6−3.8 wt %) with similar surface area (1100−1400 m^2 g^{-1}).[43,51−53] Figure 8 shows the variation of the maximum hydrogen capacity for several MOFs and MILs

(51) Liu, Y.; Eubanck, J. F.; Cairns, E. J.; Eckert, J.; Kravtsov, V. C.; Luebke, R.; Eddaoudi, M. *Angew. Chem., Int. Ed.* **2007**, *46*, 3278–3283.
(52) Férey, G.; Latroche, M.; Serre, C.; Millange, F.; Loiseau, T.; Percheron-Guegan, A. *Chem. Commun.* **2003**, *24*, 2976–2977.
(53) Volkringer, C.; Meddouri, M.; Loiseau, T.; Guillou, N.; Marrot, J.; Férey, G.; Haouas, M.; Taulelle, F.; Audebrand, N.; Latroche, M. *Inorg. Chem.* **2008**, *47*, 11892–11901.

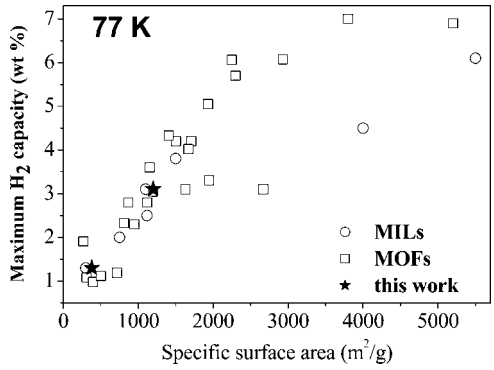

Figure 8. Correlation between the maximum hydrogen capacity at 77 K and specific surface area for different MOFs (□) and MILs (○) materials taken from the literature.[43,52,54−56] The results obtained in this work are also plotted (★).

materials taken from references[43,52,54−56] together with the present results. Considering that, as already reported for nanostructured carbon/metals composite,[47] the contribution of Pd nanoparticles during the hydrogen physisorption process is negligible at low temperatures, the textural changes induced by Pd insertion in MIL-100(Al)/Pd composite support the observed loss of excess hydrogen sorption.

A completely different behavior is observed at room temperature. The excess hydrogen sorption of MIL-100(Al) (0.19 wt % at 4 MPa) is almost doubled to 0.35 wt % for the composite. This can be explained by the steep increase in hydrogen uptake at low pressure, which can be attributed to the formation of Pd hydride. It is well-known that bulk Pd quickly absorbs hydrogen at room temperature and forms the β-hydride ($PdH_{0.6}$) at pressure below 0.1 MPa.[57] Consequently, similar formation of β-hydride occurs in the Pd nanoparticles embedded in MIL-100(Al), as clearly proven by in situ XRD (Figure 7). The formation of the Pd β-hydride is complete at 4.5 kPa hydrogen pressure. At the same pressure, the excess hydrogen adsorbed in pristine MIL-100(Al) is almost negligible (Figure 6b). Therefore, the hydrogen uptake value at 0.1 MPa as measured by PCI can be endorsed to the formation of Pd hydride. Under this assumption, the calculated H/Pd ratio for the nanoparticles of Pd hydride is approximately 1, a value higher than the commonly reported 0.6 H/Pd for microcrystalline Pd,[57] which is reduced to 0.3−0.4 H/Pd when downsizing the metal size to several nanometers.[58] For the sake of comparison, Figure 6b contains an additional PCI curve (dashed line) calculated from the sum of the amount of H_2 required for the formation of the bulk β-Pd hydride (H/Pd = 0.62 and 0.73 at 0.001 and 1 MPa, respectively[57]) and the amount of physisorbed H_2 by the Pd-free MIL-100(Al). In our case, a "spillover" effect might take place between the Pd nanoparticles and the MIL-100(Al) pore networks during the hydrogen sorption and might explain the observed increase of the capacity. The presence of confined Pd nanoparticles might promote the dissociation of molecular hydrogen on the surface of metal followed by diffusion of monatomic hydrogen in the porosity of the host metal-organic framework, as already observed for other composites.[47,59−61]

Conclusions

In conclusion, Pd nanoparticles embedded in the metal-organic framework MIL-100(Al) were successfully synthesized by a chemical wetting method. The corresponding MIL-100(Al)/Pd composite shows one of the highest metal contents (10 wt %) without degradation of the porous host. Moreover, most of the highly dispersed Pd nanoparticles (mean size 2.5 nm) are located within the pores of MIL-100(Al). This changes the textural properties with a loss of specific surface area and of total and micropore volumes. The loss of excess hydrogen storage at low temperature can be correlated with the decrease of the specific surface area and pore volume after Pd impregnation. At ambient temperature, the hydrogen uptake in the composite is almost twice that of the pristine material. This can be attributed to the formation of Pd hydride, as clearly proven by in situ XRD. However, this increase can only partially be accounted for by the Pd hydride formation, and a "spillover" mechanism may promote the dissociation of molecular hydrogen on the surface of metal nanoparticles and a further diffusion of monatomic hydrogen into the porosity of the host metal-organic framework.

Acknowledgment. This work received funding from the European Community's Sixth Framework Program through a Marie Curie Research Training Network (MRTN-CT-2004-512443) and from the French ANR funding agency through the MATHYSSE project (Contract no. ANR-07-PANH-007-01). The authors would like to thank Diana Dragoe from ICMPE, Thiais for ICP-OES chemical characterisations.

JA9084995

(54) Zhao, D.; Yuan, D.; Zhou, H. C. *Energy Environ. Sci.* **2008**, *1*, 222–235.
(55) Koh, K.; Wong-Foy, A. G.; Matzger, A. J. *J. Am. Chem. Soc.* **2009**, *131*, 4184–4185.
(56) Yan, Y.; Lin, X.; Yang, S.; Blake, A. J.; Dailly, A.; Champness, N. R.; Hubberstey, P.; Schröder, M. *Chem. Commun* **2009**, *1025*, 1027.
(57) Frieske, H.; Wicke, E. *Ber. Bunsen-Ges. Phys. Chem.* **1973**, *77*, 48–52.
(58) Pundt, A.; Kirchheim, R. *Annu. Rev. Mater. Res.* **2006**, *36*, 555–608.
(59) Wang, L.; Yang, R. T. *Energy Environ. Sci.* **2008**, *1*, 268–279.
(60) Yang, R. T.; Wang, Y. *J. Am. Chem. Soc.* **2009**, *131*, 4224–4226.
(61) Contescu, I. C.; Brown, C. M.; Liu, Y.; Bhat, V. V.; Gallego, N. C. *J. Phys. Chem. C* **2009**, *113*, 5886–5890.